Anti-dispersion in flows in leaky channels

Yiming Gan, Yisen Guo, John H Thomas, Kimberly A Boster, Jessica K Shang, and Douglas H Kelley
Department of Mechanical Engineering, University of Rochester.
(Dated: January 12, 2026)

Solute transport in a channel has important implications in industrial processes, biomechanics, and drug delivery. When flow is driven down a channel by a pressure gradient, solute is spread axially by shear and laterally by molecular diffusion. The combination causes the effective axial diffusivity to exceed the molecular diffusivity, a phenomenon known as Taylor dispersion. Here we show, however, that if the channel walls are permeable to the fluid but not to the solute, solute in the channel can be consolidated, making the effective axial diffusivity negative, a phenomenon we call "anti-dispersion." We present a theoretical model, with numerical validation, to study anti-dispersion, demonstrating that it occurs both with boluses of solute and with moving solute fronts. We determine the conditions in which anti-dispersion exceeds dispersion: high dimensionless permeability, moderate dimensionless flow speed, and concentration gradients that are not too steep. Our findings may inform understanding of biological circulation systems and design of systems for controlling solute concentration, as in drug delivery and desalination.

Considering a bolus of solute moving through a long, narrow channel in steady, pressure-driven, viscous (Poiseuille) flow, Taylor [1] demonstrated that shear spreads solute and generates sharp concentration gradients perpendicular to the flow direction, which are rapidly smoothed out by diffusion across the channel's narrow width. The combination of shear and diffusion drives rapid mixing, increases entropy, and widens the bolus more quickly than either process could do alone — a phenomenon known as Taylor dispersion [1, 2]. The rate at which a bolus spreads, or equivalently, the effective diffusivity, is increased by the greatest factor for a low-diffusivity, large-molecular-weight solute, which otherwise diffuses slowly. Taylor dispersion, in simplest form, occurs in channels with impermeable walls.

However, solutes are often transported along channels whose walls are semipermeable, blocking solute molecules but allowing fluid to leak in or out of the channel, like a sieve. For example, water purification and desalination depend on reverse osmosis through semipermeable membranes [3, 4]. The phospholipid bilayers that constitute most cell membranes typically block large molecules but have embedded aquaporin proteins which allow water to easily cross the membrane [5]. In capillaries, water leaks through the walls into the surrounding tissue [6], while cells and large molecules in the blood are retained. Similarly, in perivascular spaces that surround blood vessels in the brain, cerebrospinal fluid leaks into surrounding tissue but large particles do not [7, 8]. If fluid leaks out through channel walls, flow speed within the channel drops as fluid moves downstream. The resulting velocity gradient affects solute transport and dispersion. Although it is well known that a porous (not semipermeable) wall reduces Taylor dispersion [9], to our knowledge, no study has discussed the potential for semipermeable walls to concentrate and narrow a solute bolus.

In this Letter, we report a phenomenon opposite to Taylor dispersion: for flow in a channel with semipermeable walls, a bolus can narrow and become increasingly concentrated, so that the solute becomes less mixed and its concentration less uniform. The effective diffusivity is negative, in contrast to ordinary diffusivity, which is prohibited from being negative by the second law of thermodynamics. We derive a reduced-order model to demonstrate this "anti-dispersion" effect, and we validate the model through three-dimensional simulations. We also find that concentration gradients experience anti-dispersion, as boluses do. We explore the range of conditions in which anti-dispersion occurs. Our findings could enhance studies of biological transport, microfluidic device design, and the development of medical applications, such as the design of catheters for drug delivery.

We consider the flow in a narrow channel between two infinite, parallel, semipermeable plates, as illustrated in Fig. 1. We assume the flow to be laminar, steady, and fully-developed. The channel has width $2h$ and length L. We consider the case in which $\varepsilon = h/L \ll 1$, so we can determine the flow analytically using lubrication theory, in which the continuity and momentum equations are

$$\frac{\partial u}{\partial x} + \frac{\partial v}{\partial y} = 0, \quad \frac{\partial p}{\partial x} = \mu \frac{\partial^2 u}{\partial y^2}, \quad \frac{\partial p}{\partial y} = 0, \tag{1}$$

where x and y are the axial and transverse coordinates, u and v are the corresponding velocity components, p is the pressure, and μ is the dynamic viscosity. The pressure is

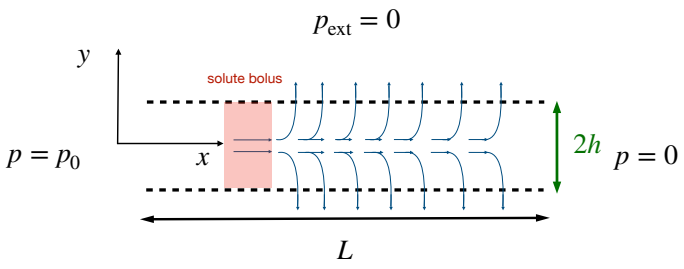

FIG. 1. A fluid-filled channel of length L, with semipermeable walls at $y = h$ and $y = -h$. Steady pressure $p_0 > 0$ is applied at the left end of the channel, driving axial flow within the channel and driving fluid, but not solute, through the wall.

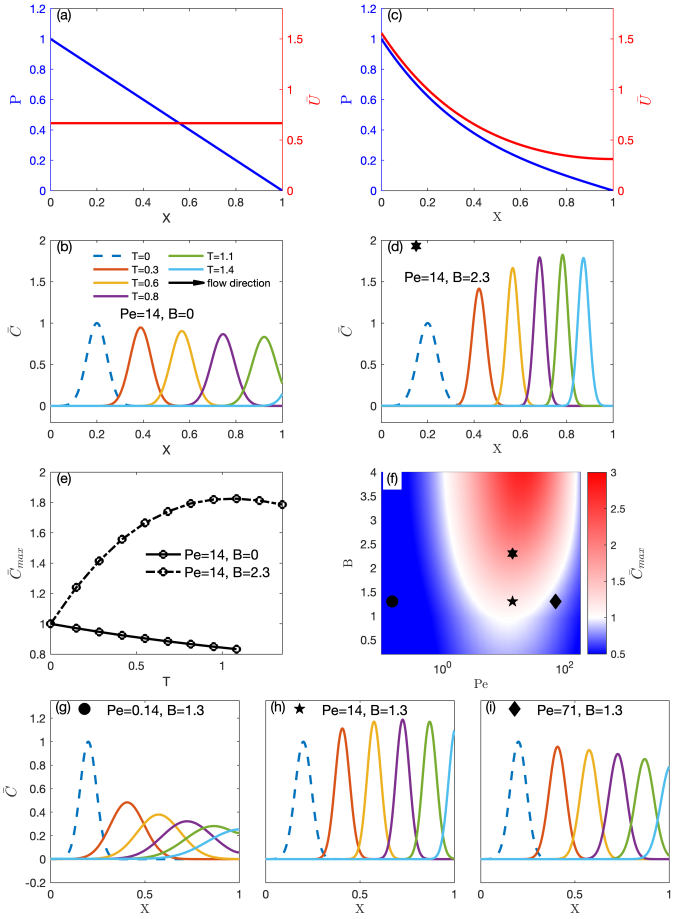

FIG. 2. Dispersion and anti-dispersion of solute boluses in channels ($\varepsilon = 0.002$). **a–b,** With impermeable walls ($B = 0$), the dimensionless pressure P drops linearly with dimensionless position X, and the dimensionless axial mean velocity $\bar{U}$ is uniform; over dimensionless time T, the profile of the dimensionless concentration $\bar{C}$ of a bolus becomes wider and shorter. **c–d,** With semipermeable walls ($B = 2.3$), both the slope of P and value of $\bar{U}$ decrease with X; the profile of $\bar{C}$ becomes narrower and taller over time. See also Supplemental Video 1 [32]. **e,** The normalized maximum concentration $\bar{C}_{\max}$ decreases with time for $B = 0$ but increases with time for $B = 2.3$. **f,** $\bar{C}_{\max}$ at $T = 1.2$ is large when B is large and Pe is moderate. **g–i,** With semipermeable walls ($B = 1.3$) and very slow ($Pe = 0.14$) or very fast ($Pe = 71$) flow, the profile of $\bar{C}$ widens over time. But with moderate flow ($Pe = 14$), $\bar{C}$ narrows over time. See also Supplemental Video 2 [32].

$p_0 > 0$ at the inlet and $p = 0$ at the outlet. The walls are no-slip boundaries ($u_{y=h} = u_{y=-h} = 0$) but they allow fluid to exit according to the Starling filtration law

$$v_{y=h} = -v_{y=-h} = \mathcal{L}_p(p - p_{\text{ext}}) \ , \tag{2}$$

where $\mathcal{L}_p$ is the hydraulic conductivity of the porous wall (linearly proportional to the wall permeability) and $p_{\text{ext}} = 0$ is the pressure external to the porous wall. We neglect osmotic effects.

Defining a characteristic velocity $u_0 = p_0 h\varepsilon/(2\mu)$ and the dimensionless variables $X = x/(h/\varepsilon)$, $Y = y/h$, $P = p/p_0$, $U = u/u_0$, and $V = v/(u_0\varepsilon)$, Eqs. 1 and 2 lead to $P = -\sinh(B(X-1))/\sinh(B)$, where the dimensionless quantity $B \equiv \sqrt{3\mathcal{L}_p\mu/h/\varepsilon}$, which varies with the ratio of the hydraulic conductivity of the leaky wall to that of the channel itself, is an important parameter. The corresponding velocity field is

$$U = \frac{dP}{dX}(Y^2 - 1) \ , \ V = -\frac{d^2P}{dX^2}\left(\frac{Y^3}{3} - Y\right). \tag{3}$$

Mathematical details are presented in the Appendix. Dejam and Hassanzade [10] derived an analytical solution that characterizes the effect of a semipermeable wall on dispersion, but the flow field considered in their model is one-dimensional and thereby independent of the axial direction. Griffiths et al. [11] considered axial flow gradients, but in the absence of semipermeability.

The advection-diffusion equation governing solute transport in the channel is

$$\frac{\partial C}{\partial t} + u\frac{\partial C}{\partial x} + v\frac{\partial C}{\partial y} = D\left(\frac{d^2C}{dx^2} + \frac{d^2C}{dy^2}\right), \tag{4}$$

where C is the dimensionless solute concentration ($0 \le C \le 1$), t is time, and D is the diffusivity of the solute. Defining the scaled time $T = t/t_0 = t/(h\varepsilon^{-1}u_0^{-1})$ gives

$$\frac{\partial C}{\partial T} + U\frac{\partial C}{\partial X} + V\frac{\partial C}{\partial Y} = \frac{1}{Pe}\left(\varepsilon\frac{d^2C}{dX^2} + \frac{1}{\varepsilon}\frac{d^2C}{dY^2}\right), \tag{5}$$

where $Pe = u_0 h/D$ is the Péclet number, another important dimensionless parameter (independent of B). Performing a Reynolds decomposition, we let $C = \bar{C}(X,T) + C'(X,Y,T)$ and $U = \bar{U}(X) + U'(X,Y)$, where $\bar{C}(X,T)$ and $\bar{U}(X)$ are the cross-sectional averages of concentration and axial velocity, respectively. Considering times $t_0 \gg h^2/D$, assuming that transverse solute transport is dominated by diffusion ($\varepsilon Pe \ll 1$), and averaging both sides of Eq. 5 leads to

$$\frac{\partial \bar{C}}{\partial T} + \bar{U}\frac{\partial \bar{C}}{\partial X} = \frac{\varepsilon}{Pe}(1 + \mathcal{F}\bar{U}^2Pe^2)\frac{d^2\bar{C}}{dX^2} + \frac{1}{\varepsilon Pe}\frac{\partial C'}{\partial Y}\bigg|_{Y=1}, \tag{6}$$

where $\mathcal{F} = 2/105$ [11]. The third term in Eq. 6 describes the enhanced diffusion in the axial direction due to Taylor dispersion [2], and the last term describes the solute transport through the semipermeable walls.

At the semipermeable wall at $Y = 1$, the solute flux is

$$J = V_{Y=1}(\bar{C} + C') - \frac{1}{\varepsilon Pe}\frac{\partial C'}{\partial Y}\bigg|_{Y=1}, \tag{7}$$

where $V_{Y=1}$ is the transverse flow velocity at the wall. The solute flux at the wall at $Y = -1$ is given by a similar expression. For a solute that cannot permeate the wall, $J = 0$. Applying this condition to Eq. 6 and assuming $\bar{C} \gg C'$, we have

$$\frac{\partial \bar{C}}{\partial T} + \bar{U}\frac{\partial \bar{C}}{\partial X} = \frac{\varepsilon}{Pe}(1 + \mathcal{F}\bar{U}^2Pe^2)\frac{d^2\bar{C}}{dX^2} + V_{Y=1}\bar{C}. \tag{8}$$

If a bolus of solute (a localized region of high concentration) is present, the last term in Eq. 8 is positive, acting as a source that increases concentration. Meanwhile, the second (advection) term narrows the bolus due to a negative axial velocity gradient, as described by Eq. 3. The third term accounts for Taylor dispersion, which tends to broaden the bolus and reduce concentration.

We set zero concentration at the inlet ($C|_{X=0} = 0$) and zero concentration gradient at the outlet ($d\bar{C}/dX|_{X=1} = 0$), allowing solute efflux through pure advection. We assume the initial concentration to have a Gaussian profile, $C_{T=0} = C_0 \exp(-(X - X_0)^2/(2\sigma^2))$, where $C_0 = 1$, $X_0 = 0.2$, and $\sigma = 0.09$. Equation 8 is solved in the frequency domain using a Laplace transform, and mapped to the time domain using a numerical inverse Laplace transform and a spectral method in space [12, 13].

When the wall is impermeable ($B = 0$), the pressure gradient and axial velocity are uniform from inlet to outlet (Fig. 2a). In that case, over time, the bolus's width increases and its maximum concentration decreases, both due to Taylor dispersion (Fig. 2b). However, when the wall is semipermeable ($B = 2.3$), the pressure gradient is steeper near the inlet than near the outlet, causing a negative axial velocity gradient (Fig. 2c). In that case, over time, the bolus's width decreases and its maximum concentration increases (Fig. 2d), a behavior we call "anti-dispersion." Figure 2e shows that the maximum concentration decreases over time when $B = 0$ but increases over time when $B = 2.3$. Eventually, the bolus becomes so narrow that dispersion overcomes anti-dispersion and the peak concentration begins to drop again.

In both of those cases, we considered flows with $Pe = 14$, but the results depend on Pe as well as B. For example, choosing $B = 1.3$ but considering very slow flow ($Pe = 0.14$) or very fast flow ($Pe = 71$), we observed boluses spreading over time, not narrowing (Fig. 2g,i), while choosing a moderate flow speed ($Pe = 14$) lead to anti-dispersion (Fig. 2h). Figure 2f shows how the maximum concentration $\bar{C}_{\max}$ at time $T = 1.2$ varies with both Pe and B. Increasing B increases $\bar{C}_{\max}$ (promotes anti-dispersion) because a leakier channel leads to flows with steeper velocity gradients that compress the bolus. Increasing Pe from values near zero to values of order unity increases $\bar{C}_{\max}$ and promotes anti-dispersion, but increasing Pe further decreases $\bar{C}_{\max}$ and hinders anti-dispersion. That finding is consistent with Eq. 8: anti-dispersion occurs when Pe is large enough for the velocity gradient to be steep but not so large that Taylor dispersion overwhelms anti-dispersion. Our analytic model was validated with numerical simulations (see the Appendix).

We now examine the case of a uniform boundary outflow speed $V_{Y=1}$ (instead of uniform hydraulic conductivity $\mathcal{L}_p$). Assuming that the average concentration profile is Gaussian with characteristic width σ, we have $\partial^2\bar{C}/\partial X^2 = -\bar{C}/\sigma^2$ at $X = X_0$, where the concentration is maximum. Equation 8 then becomes

$$\left.\frac{D\bar{C}}{DT}\right|_{X=X_0} = M\bar{C}, \tag{9}$$

where D/DT is the material derivative and $M = -\varepsilon\sigma^{-2}Pe^{-1}(1 + \mathcal{F}\bar{U}^2Pe^2) + V_{Y=1}$. Peak concentration decreases and the bolus widens when $M < 0$; peak concentration increases and the bolus narrows when $M > 0$. The value of M depends on $\bar{U}(X)$ and $\sigma(X, T)$. We consider here $M_0 = -\varepsilon\sigma_0^{-2}Pe^{-1}(1 + \mathcal{F}\langle\bar{U}\rangle^2Pe^2) + V_{Y=1}$, which is independent of space and time, where σ_0 is the width of the initial bolus, $\langle\bar{U}\rangle = \int_{X=0}^{X=1}\bar{U}(X)\,dX$ is the axial velocity averaged in the axial direction, and $V_{Y=1} = B_{X=0}^2/2$. The first term on the right depends on σ, $\bar{U}$, and Pe.

Alternatively, we can write Eq. 9 as

$$\left.\frac{D\bar{C}}{DT}\right|_{X=X_0} = \frac{\varepsilon}{Pe}\frac{D_{\text{eff}}}{D}\frac{\partial^2\bar{C}}{\partial X^2}, \tag{10}$$

where $D_{\text{eff}}/D = -Pe\sigma^2M/\varepsilon$, is the ratio between the effective diffusivity and the inherent diffusivity of the solute, where a negative value indicates anti-dispersion. Again, we consider $D_{\text{eff}0}/D = -Pe\sigma_0^2M_0/\varepsilon$, which is independent of space and time.

If $V_{Y=1}$ is uniform, conductivity must vary spatially:

$$\mathcal{L}_p(X) = \frac{\mathcal{L}_p|_{X=0}}{(B_{X=0}^2/2)X^2 + (\alpha - 1 - B_{X=0}^2/2)X + 1}\,, \tag{11}$$

where αp_0 is the pressure at the outlet ($0 < \alpha < 1$).

In this case, $\mathcal{L}_p$ increases with X, P is a parabolic function of X, and $\bar{U}$ is a linear function of X (Fig. 3a,b). Figure 3c shows $\bar{C}_{\max}$ at $T = 1.2$ for different values of B and Pe. The regime where anti-dispersion dominates can be determined analytically by the sign of M and approximated by the sign of M_0. The region in Fig. 3d where $M_0 > 0$ approximately overlaps the region where anti-dispersion dominates. Figure 3e shows that $\bar{C}_{\max}$ increases with σ. Again, the region where $M_0 > 0$ in Fig. 3f overlaps with the region where anti-dispersion dominates.

Finally, we move from boluses to examine the case in which the concentration at the inlet is suddenly altered according to a step function, as at the beginning of a steady injection of solute, producing a moving concentration front. With nearly impermeable walls ($B = 0.1$), the profile of $\bar{C}$ is smoothed over time but remains mostly flat on both sides of the front (Fig. 4a). However, with semipermeable walls ($B = 3.2$), the profile of $\bar{C}$ curves upward over time as solute accumulates near the front (Fig. 4b). The peak concentration occurs at the front and exceeds the inlet concentration. Figure 4c shows how $\bar{C}_{\max}$ varies over time with different values of B, remaining nearly constant when B is small but growing and saturating when B is large. Interestingly, the largest values of $\bar{C}_{\max}$ far exceed those observed for boluses (Fig. 2e). That observation is consistent with our

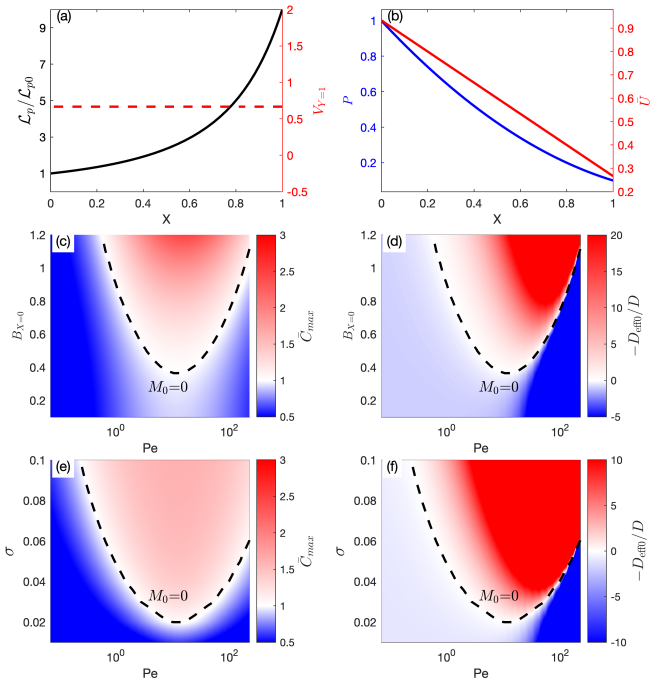

FIG. 3. Dispersion and anti-dispersion in channels ($\varepsilon = 0.001$) with uniform outflow through the walls. **a,** If the wall's conductivity $\mathcal{L}_p(X)$ obeys Eq. 11, the outflow velocity $V_{Y=1}$ is constant. Here, $\alpha = 0.1$. **b,** In this case, P is parabolic, and $\bar{U}$ is linear. (**c**) $\bar{C}_{\max}$ at $T = 1.2$ is large when $B_{X=0}$ is large and Pe is moderate. To a good approximation, $\bar{C}_{\max} > 1$ where $M_0 > 0$. **d,** The normalized effective diffusivity $-D_{\text{eff}0}/D$ is large when $B_{X=0}$ is large and Pe is moderate. To a good approximation, $-D_{\text{eff}0}/D > 1$ where $M_0 > 0$. **e,** $\bar{C}_{\max}$ is large when σ is large and Pe is moderate. To a good approximation, $\bar{C}_{\max} > 1$ where $M_0 > 0$. **f,** $-D_{\text{eff}0}/D$ is large when σ is large and Pe is moderate. $-D_{\text{eff}0}/D > 1$ where $M_0 > 0$.

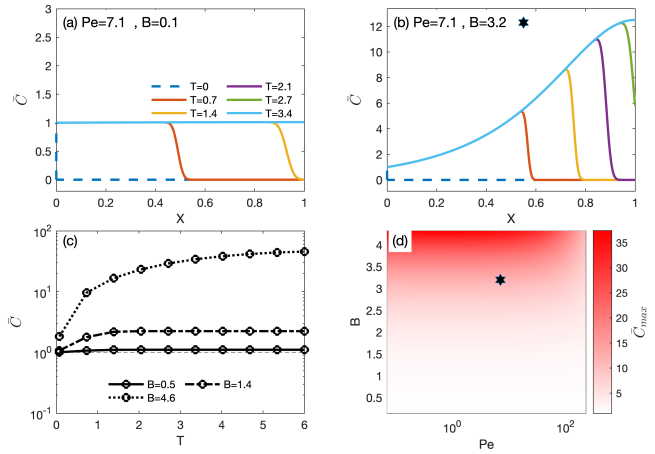

FIG. 4. Anti-dispersion of moving concentration fronts ($\varepsilon = 0.001$). **a,** With nearly impermeable walls ($B = 0.1$), the profile of $\bar{C}$ is smoothed at the front over time but remains flat elsewhere. **b,** In a leaky channel with semipermeable walls ($B = 3.2$), the profile of $\bar{C}$ curves upward over time. See also Supplemental Video 3 [32]. **c–d,** $\bar{C}_{\max}$ at $T = 1.2$ increases and saturates over time, growing more when B is larger but showing little variation with Pe. A star marks the parameter values considered in (b).

finding, above, that anti-dispersion is stronger for wide boluses (large σ); the semi-infinite region of high concentration behind a moving front can be understood as a very wide bolus. Large B consistently leads to large $\bar{C}_{\max}$, but for moving fronts, altering Pe has little effect (Fig. 4d). That observation is consistent with the fact that Taylor dispersion has little effect, since C is nearly uniform except near the front. For some values of B, concentration gradients near the front become so steep that, eventually, dispersion overcomes anti-dispersion and the peak concentration begins to drop.

We have shown that solute traveling along a channel with semipermeable walls can become less mixed over time, with high-concentration regions becoming more concentrated and low-concentration regions becoming less so. This "anti-dispersion" is possible because semipermeable walls leak fluid but not solute. For a bolus, anti-dispersion is strong when B is large (leakier, longer, and narrower channels), the Péclet number Pe is moderate, and concentration gradients are not too steep. Anti-dispersion is driven by the axial velocity gradient in the channel, which scales as B^2Pe; therefore, its effects are negligible when axial transport is dominated by diffusion ($Pe \ll 1$). Its effects are also negligible when $Pe \gg 1$ because of strong Taylor dispersion.

We varied the permeability of the wall to achieve uniform fluid leakage along the channel (Figure 3a), enabling us to derive an analytical expression for the effective diffusivity of a Gaussian-profiled bolus. When the effective diffusivity becomes negative, the bolus narrows and becomes more concentrated (Figure 3d). Notably, the maximum concentration increases with the characteristic bolus width σ, indicating that a broader bolus is more prone to concentration than dispersion (Figure 3f). This is consistent with our steady-injection study, where the solute reaches a maximum width at steady state. For solute fronts, anti-dispersion depends less on Pe because the solute is already uniformly distributed in most places, weakening dispersion.

We expect anti-dispersion to be observable with available materials and flow parameters. For example, a membrane with 45-nm pores with wall permeability 5×10^{-7} m/Pa/s [14] would readily pass water molecules (with a radius around 0.2 nm) but block solute molecules with radius 100 nm, whose diffusivity at room temperature is about 5.6×10^{-12} m^2/s [15]. In a channel 5 mm long and 20 µm wide with peak inlet velocity 10 µm/s, $B = 1.8$ and $Pe = 35$, and we would expect to see anti-dispersion, according to Fig. 2. Due to the higher Péclet number, solutes with lower diffusivity experience more pronounced stretching and dispersion within the channel, making them more susceptible to dilution.

Anti-dispersion might be applied to drug delivery, where precise control of concentration is essential [16, 17].

For controlled drug release, Taylor dispersion can cause premature release, but combining it with anti-dispersion (by dynamically manipulating Pe) might help precisely control the drug concentration during the injection. In tumor therapy [18], anti-dispersion could reduce mixing and dilution of the drug before it reaches the target site, enhancing its effectiveness. A typical microcatheter for drug delivery has a radius of $r \sim 0.5$ mm (similar to the channel width h we considered) and a length of $L \sim 1000$ mm [19], leading to a small aspect ratio of ~ 0.0005. According to Fig. 2f, when the catheter wall has a permeability greater than $\sim 1 \times 10^{-7}$ m/Pa/s (corresponding to $B \sim 2$), a drug bolus can be concentrated through anti-dispersion during the injection at $Pe \sim 10$. The Péclet number can be tuned by adjusting the injection flow speed based on the diffusivity of the specific drug.

Anti-dispersion might also be used to separate solutes of different diffusivities, causing some solutes to experience anti-dispersion while others are dispersed. For example, to separate particles of sizes 0.1 μm and 1 μm [20], which have diffusivities differing by orders of magnitude [15], we can maintain a moderate Pe (Fig. 2h) so that the small particles undergo anti-dispersion while the large, high-Pe particles disperse (Fig. 2i).

The ability to concentrate a solute is desirable in microfluidic applications spanning industrial, biochemical, and medical settings. For example, increasing the concentration of a dilute solute could decrease the detection limit and increase the signal-noise-ratio in bioassay tests [21, 22], such as pregnancy and COVID-19 tests [23, 24]. A coronavirus particle has a diameter of ~ 100 nm, much larger than that of a water molecule, making it possible to anti-disperse using a semipermeable membrane in the assay. As the antigen solution moves from the sample pad to the test line under capillary force, the process can be modeled as a moving concentration front (Figure 4d), where anti-dispersion occurs despite the relatively high flow speed in the assay (~ 0.1 mm/s).

Existing approaches for concentrating solutes can be divided into active techniques (manipulating particles or species with an externally applied force, such as electric, magnetic, acoustic, or optical) and passive techniques (e.g., diffusiophoresis, evaporation, or filtration). Here we describe how a solute can be concentrated in certain lateral-flow scenarios. The framework we present for predicting anti-dispersion can be used to design microfluidic devices that concentrate a solute. Those devices typically have a larger ϵ (~ 0.01) than catheters [14], implying that a higher permeability ($L_p > 1 \times 10^{-6}$ m/Pa/s) is required to anti-disperse a bolus there.

Many channels in biological systems have slippery walls or are filled with porous material. In either case, the shear in the flow is reduced, diminishing the effect of Taylor dispersion and thus promoting anti-dispersion. When the channel is filled with porous material, both fluid and solute must pass through small pores, and the shear is determined by the characteristic width of these narrower pathways, resulting in much weaker dispersion. On the other hand, the hydraulic conductivity of a porous channel is smaller than that of an open channel, leading to a higher value of B and thereby enhancing anti-dispersion.

Bounded by permeable tissue, a perivascular space surrounding a penetrating artery in the brain is a pathway for cerebrospinal fluid flow. In mice, the characteristic width of such a perivascular space is ~ 5 μm, the length is ~ 1000 μm, and the speed is ~ 1 μm/s [25]. Gaps in the wall have width ~ 20 nm [26, 27], making it permeable to smaller solutes only. These parameter values are likely within the regime of anti-dispersion. Measurement of flow in these spaces using particle tracking velocimetry is not currently feasible, however. Moreover, in vivo measurement of wall permeability is prevented by the optical diffraction limit. However, small-molecule tracer experiments are currently available, and using them to quantify dispersion and anti-dispersion in a perivascular space might reveal the permeability of its outer wall and the velocity of the cerebrospinal fluid within [28, 29].

Our study has caveats. First, osmotic pressure — proportional to the solute concentration [30] — has been neglected in our model and in related studies [10]. This neglect is justified when the osmotic pressure is much smaller than the applied pressure driving the flow, particularly in cases involving dilute solutes, viscous flows, or channels with high outlet resistance. Although developing a corresponding reduced model is challenging and beyond the scope of this study, osmotic pressure should be incorporated in a future study. Second, our model considers a two-dimensional channel for simplicity. However, the model can be readily extended to other geometries, such as circular or annular channels. It can also be adapted to accommodate different boundary conditions.

ACKNOWLEDGMENTS

We acknowledge insightful discussions with Ibrahim Mohammad, Mohammad Vaezi, Aditya Ranjan, Wenjie Zang, Yuxuan Liu, and James McGrath. This work was supported by the US National Center for Complementary and Integrative Health (grant no. R01AT012312), the BRAIN Initiative of the US National Institutes of Health under (grant no. U19NS128613), and the US National Science Foundation CAREER Program (grant no. CBET-2143702).

[1] G. I. Taylor, The dispersion of matter in turbulent flow through a pipe, Proceedings of the Royal Society of London. Series A. Mathematical and Physical Sciences **223**, 446 (1954).

[2] R. Aris, On the dispersion of a solute in a fluid flowing through a tube, Proceedings of the Royal Society of London. Series A. Mathematical and Physical Sciences **235**, 67 (1956).

[3] G. Belfort, Fluid mechanics in membrane filtration: recent developments, Journal of Membrane science **40**, 123 (1989).

[4] M. Shahbabaei and D. Kim, Advances in nanofluidics for water purification and filtration: molecular dynamics (md) perspective, Environmental Science: Nano **8**, 2120 (2021).

[5] N. MacAulay, Molecular mechanisms of brain water transport, Nature Reviews Neuroscience **22**, 326 (2021).

[6] K. Huang, L. Pan, and R.-H. Yoon, A capillary flow model for filtration, Minerals Engineering **115**, 88 (2018).

[7] J. J. Iliff, H. Lee, M. Yu, T. Feng, J. Logan, M. Nedergaard, H. Benveniste, *et al.*, Brain-wide pathway for waste clearance captured by contrast-enhanced mri, The Journal of clinical investigation **123**, 1299 (2013).

[8] D. H. Kelley and J. H. Thomas, Cerebrospinal fluid flow, Annual review of fluid mechanics **55**, 237 (2023).

[9] M. Dejam and H. Hassanzadeh, The role of a porous wall on the solute dispersion in a concentric annulus, Physics of Fluids **33** (2021).

[10] M. Dejam and H. Hassanzadeh, Dispersion in a slit with crossflow filtration through a porous wall, Physics of Fluids **36** (2024).

[11] I. Griffiths, P. Howell, and R. Shipley, Control and optimization of solute transport in a thin porous tube, Physics of Fluids **25** (2013).

[12] J. Valsa and L. Brančik, Approximate formulae for numerical inversion of laplace transforms, International Journal of Numerical Modelling: Electronic Networks, Devices and Fields **11**, 153 (1998).

[13] J. P. Boyd, *Chebyshev and Fourier spectral methods* (Courier Corporation, 2001).

[14] A. T. Salminen, J. Zhang, G. R. Madejski, T. S. Khire, R. E. Waugh, J. L. McGrath, and T. R. Gaborski, Ultrathin dual-scale nano- and microporous membranes for vascular transmigration models, Small **15**, 1804111 (2019).

[15] A. Einstein, Über die von der molekularkinetischen theorie der wärme geforderte bewegung von in ruhenden flüssigkeiten suspendierten teilchen, Annalen der physik **4** (1905).

[16] A. I. Minchinton and I. F. Tannock, Drug penetration in solid tumours, Nature Reviews Cancer **6**, 583 (2006).

[17] J. Alaminos-Quesada, C. Gutiérrez-Montes, W. Coenen, and A. Sánchez, Effects of buoyancy on the dispersion of drugs released intrathecally in the spinal canal, Journal of fluid mechanics **985**, A20 (2024).

[18] L. R. Mashiku, J. P. Ndenda, R. Maghembe, and S. Shaw, Impact of drug dispersion on tumor-effector dynamics during combined chemo-immunotherapy with sensitivity analysis, Applied Mathematical Modelling **134**, 148 (2024).

[19] T. Wattanasatesiri, J. W. Chung, T. W. Choi, H.-C. Kim, M. Lee, and S. Hur, Shaping the tip of microcatheters for superselective catheterization: steam vs. manual methods, Diagnostic and Interventional Radiology **26**, 456 (2020).

[20] S. Shen, C. Tian, T. Li, J. Xu, S.-W. Chen, Q. Tu, M.-S. Yuan, W. Liu, and J. Wang, Spiral microchannel with ordered micro-obstacles for continuous and highly-efficient particle separation, Lab on a Chip **17**, 3578 (2017).

[21] K. M. Koczula and A. Gallotta, Lateral flow assays, Essays in biochemistry **60**, 111 (2016).

[22] A. Gupta, S. Shim, and H. A. Stone, Diffusiophoresis: from dilute to concentrated electrolytes, Soft Matter **16**, 6975 (2020).

[23] W. C. Mak, V. Beni, and A. P. Turner, Lateral-flow technology: From visual to instrumental, TrAC Trends in Analytical Chemistry **79**, 297 (2016).

[24] J. Budd, B. S. Miller, N. E. Weckman, D. Cherkaoui, D. Huang, A. T. Decruz, N. Fongwen, G.-R. Han, M. Broto, C. S. Estcourt, *et al.*, Lateral flow test engineering and lessons learned from covid-19, Nature Reviews Bioengineering **1**, 13 (2023).

[25] B. Bedussi, M. Almasian, J. de Vos, E. VanBavel, and E. N. T. P. Bakker, Paravascular spaces at the brain surface: Low resistance pathways for cerebrospinal fluid flow, J Cerebr Blood F Met **38**, 719 (2017).

[26] T. Koch, V. Vinje, and K.-A. Mardal, Estimates of the permeability of extra-cellular pathways through the astrocyte endfoot sheath, Fluids Barr. CNS **20**, 20 (2023).

[27] M. X. Wang, L. Ray, K. F. Tanaka, J. J. Iliff, and J. Heys, Varying perivascular astroglial endfoot dimensions along the vascular tree maintain perivascular-interstitial flux through the cortical mantle, Glia **69**, 715 (2021).

[28] K. A. Boster, S. Cai, A. Ladrón-de Guevara, J. Sun, X. Zheng, T. Du, J. H. Thomas, M. Nedergaard, G. E. Karniadakis, and D. H. Kelley, Artificial intelligence velocimetry reveals in vivo flow rates, pressure gradients, and shear stresses in murine perivascular flows, Proceedings of the National Academy of Sciences **120**, e2217744120 (2023).

[29] M. Raissi, A. Yazdani, and G. E. Karniadakis, Hidden fluid mechanics: Learning velocity and pressure fields from flow visualizations, Science **367**, 1026 (2020).

[30] G. N. Lewis, The osmotic pressure of concentrated solutions, and the laws of the perfect solution., Journal of the American Chemical Society **30**, 668 (1908).

[31] J. P. Gleeson and H. A. Stone, Taylor dispersion in electroosmotic flows with random zeta potentials, in *Technical Proceedings of the 2004 NSTI Nanotechnology Conference and Trade Show* (Citeseer, 2004) pp. 375–378.

[32] See Supplemental Material at [URL] for further details and results .

[33] Matlab scripts to produce the results presented in this article are openly available at https://github.com/Germaize/Anti_Dispersion
.

APPENDIX

1. Derivation of the reduced-order model

a. The flow field

Under lubrication theory, the pressure differences in the y direction are negligible in the two-dimensional Navier–Stokes equations, leading to

$$\frac{\partial u}{\partial x}+\frac{\partial v}{\partial y}=0,\ \frac{\partial p}{\partial x}=\mu\frac{\partial^2 u}{\partial y^2},\quad \frac{\partial p}{\partial y}=0, \tag{12}$$

where u is the flow velocity in the axial direction (x), v is the flow velocity in the transverse direction (y) and p is the pressure. Solving Eq. 12 with a no-slip boundary condition at the wall gives

$$u=\frac{1}{2\mu}\frac{dp}{dx}(y^2-h^2),\ v=\frac{1}{\mu}\frac{d^2p}{dx^2}(h^2\frac{y}{2}-\frac{y^3}{6})\ . \tag{13}$$

The velocity at the permeable wall ($y=h$), according to the Starling law and neglecting the osmotic component, is given by $v(y=h)=\mathcal{L}_p(p-p_{\text{ext}})$, where $\mathcal{L}_p$ is the permeability of the outer wall, and p_{ext} is the pressure outside the permeable wall. Combining the equations above, with an inlet pressure of p_0 and an outlet pressure of 0, and $p_{\text{ext}}=0$, we have

$$\mathcal{L}_p p=\frac{h^3}{3\mu}\frac{d^2p}{dx^2}\ . \tag{14}$$

For a tube with a length L, we have

$$p=p_0\frac{\sinh B(1-x/L)}{\sinh B}\ , \tag{15}$$

where $B=\sqrt{3k\mu/h}/\varepsilon$.

We can express these equations in dimensionless form, using the dimensionless quantities $T=t/t_0$, $X=x/(h/\varepsilon)$, $\varepsilon=h/L$, $Y=y/h$, $P=p/p_0$, $U=u/u_0$, $V=v/(u_0\varepsilon)$ (from the continuity equation). We define p_0 as $p_0=2\mu u_0/h\varepsilon=2\mu v_0/h\varepsilon^2$, which ensures that a prescribed pressure of p_0 will drive a velocity of u_0 at the center line (y=0) of the tube when the outer wall is impermeable. The dimensionless pressure distribution is

$$P=-\frac{\sinh(B(X-1))}{\sinh(B)}\ , \tag{16}$$

and therefore the fully resolved velocity components are

$$U=\frac{dP}{dX}(Y^2-1),\ V=-\frac{d^2P}{dX^2}(\frac{Y^3}{3}-Y)\ . \tag{17}$$

b. The advection-diffusion equation

Within the tube, the governing advection-diffusion equation is

$$\frac{\partial C}{\partial t}+u\frac{\partial C}{\partial x}+v\frac{\partial C}{\partial y}=D(\frac{d^2C}{dx^2}+\frac{d^2C}{dy^2})\ . \tag{18}$$

Letting $T=t/(h/u_0^{-1}\varepsilon^{-1})=t/t_0$, this equation has the dimensionless form

$$\frac{\partial C}{\partial T}+U\frac{\partial C}{\partial X}+V\frac{\partial C}{\partial Y}=\frac{1}{Pe}(\varepsilon\frac{d^2C}{dX^2}+\frac{1}{\varepsilon}\frac{d^2C}{dY^2})\ , \tag{19}$$

where $Pe=u_0h/D$ is the Péclet number. This equation is consistent with [31]. Using Reynolds decomposition, we express the concentration and the axial velocity as the sum of a mean term and a perturbation term,

$$C(X,Y,T)=\overline{C}(X,T)+C'(X,Y,T)\ , \tag{20}$$

$$U(X,Y)=\overline{U}(X)+U'(X,Y)\ , \tag{21}$$

where the cross-sectional average of the perturbation terms is zero.

For a two-dimensional rectangular channel, we have

$$\bar{U}(X)=-\frac{2}{3}\frac{dP}{dX},\ U'(X,Y)=-(\frac{1}{3}-Y^2)\frac{dP}{dX}\ . \tag{22}$$

Equation 19 after the decomposition reads

$$\begin{aligned}\frac{\partial\bar{C}}{\partial T}+\frac{\partial C'}{\partial T}+\bar{U}\frac{\partial\bar{C}}{\partial X}+U'\frac{\partial\bar{C}}{\partial X}+\bar{U}\frac{\partial C'}{\partial X}+U'\frac{\partial C'}{\partial X}+V\frac{\partial C'}{\partial Y}\\ =\frac{1}{Pe}(\varepsilon\frac{d^2\bar{C}}{dX^2}+\varepsilon\frac{d^2C'}{dX^2}+\frac{1}{\varepsilon}\frac{d^2C'}{dY^2})\ .\end{aligned} \tag{23}$$

In Eq. 23, the fifth term ($\bar{U}\partial C'/\partial X$) is negligible compared to the third term $\bar{U}\partial\bar{C}/\partial X$ because $C'\ll C$. Averaging Eq. 23 over the cross section, we have

$$\frac{\partial\bar{C}}{\partial T}+\bar{U}\frac{\partial\bar{C}}{\partial X}+\overline{U'\frac{\partial C'}{\partial X}}+\overline{V\frac{\partial C'}{\partial Y}}=\frac{1}{Pe}(\varepsilon\frac{d^2\bar{C}}{dX^2}+\frac{1}{\varepsilon}\frac{dC'}{dY}|_{Y=0}^{Y=1})\ , \tag{24}$$

and subtracting Eq. 24 from Eq. 23, we have

$$\begin{aligned}\frac{\partial C'}{\partial T}+U'\frac{\partial\bar{C}}{\partial X}+(U'\frac{\partial C'}{\partial X}-\overline{U'\frac{\partial C'}{\partial X}})+(V\frac{\partial C'}{\partial Y}-\overline{V\frac{\partial C'}{\partial Y}})\\ =\frac{1}{Pe}(\varepsilon\frac{d^2C'}{dX^2}+\frac{1}{\varepsilon}\frac{d^2C'}{dY^2}-\frac{1}{\varepsilon}\frac{dC'}{dY}|_{Y=0}^{Y=1})\ .\end{aligned} \tag{25}$$

The first term in this equation can be neglected when diffusion in the transverse direction has completed ($t\gg h^2/D$). The third term is much less than the second term, given that $\bar{C}\gg C'$. The fourth term, representing advection in the transverse direction, can be neglected when the transport in the transverse direction is diffusion-dominated (because the channel is narrow); The quantity $\varepsilon\partial^2C'/\partial^2X$ in the diffusion term on the right can be neglected, given that axial diffusion is negligible compared to transverse diffusion (because ε is small). Therefore, we have

$$U'\frac{\partial\bar{C}}{\partial X}=\frac{1}{\varepsilon Pe}\left(\frac{d^2C'}{dY^2}-\frac{dC'}{dY}|_{Y=0}^{Y=1}\right)\ . \tag{26}$$

Integrating Eq. 26 over y twice, we have

$$C' = \varepsilon Pe\,\bar{U}\frac{\partial \bar{C}}{\partial X}\left(\frac{Y^2}{4}-\frac{Y^4}{8}-\frac{7}{120}\right)+\frac{dC'}{dY}|_{Y=0}^{Y=1}\left(\frac{Y^2}{2}-\frac{1}{6}\right). \tag{27}$$

Note that the unknown constants in this expression were evaluated given the definition that $\int_0^1 C'dY = 0$ and $C'(Y) = C'(-Y)$ (the geometry is symmetric). Inserting this expression for C' (Eq. 27) and the expressions for U' and V (Eqs. 22) into the cross-sectionally averaged Eq. 24, the second and third unknown terms are determined to be

$$\overline{U'\frac{\partial C'}{\partial X}} = -\frac{2\bar{U}\varepsilon Pe}{105}\left(\frac{\partial \bar{U}}{\partial X}\frac{\partial \bar{C}}{\partial X}+\bar{U}\frac{\partial^2 \bar{C}}{\partial X^2}\right)-\frac{\bar{U}}{15}\frac{\partial^2 C'}{\partial X \partial Y}|_{Y=0}^{Y=1} \tag{28}$$

and

$$\overline{V\frac{\partial C'}{\partial Y}} = \varepsilon\frac{3}{35}V|_{Y=1}\bar{U}Pe\frac{\partial \bar{C}}{\partial X}+\frac{2}{5}V|_{Y=1}\frac{\partial C'}{\partial Y}|_{Y=0}^{Y=1}. \tag{29}$$

$\overline{V\partial C'/\partial Y}$ represents advection in the transverse direction, which we later prove is negligible when transport in that direction is dominated by diffusion ($\varepsilon Pe \ll 1$).

Plugging Eqs. 28 and 29 into Eq. 24, we arrive at the leading-order equation for C:

$$\begin{aligned}\frac{\partial \bar{C}}{\partial T}+\left(\bar{U}-\varepsilon Pe\frac{2}{105}\bar{U}\frac{\partial \bar{U}}{\partial X}+\frac{3\varepsilon Pe}{35}V|_{Y=1}\right)\frac{\partial \bar{C}}{\partial X}\\ +\frac{2}{5}V|_{Y=1}\frac{\partial C'}{\partial Y}|_{Y=0}^{Y=1} = \frac{\varepsilon}{Pe}(1+\frac{2}{105}\bar{U}^2Pe^2)\frac{d^2\bar{C}}{dX^2}+\\ \frac{1}{\varepsilon Pe}\frac{dC'}{dY}|_{Y=0}^{Y=1}+\frac{1}{15}\bar{U}\frac{\partial^2 C'}{\partial X\partial Y}|_{Y=0}^{Y=1}.\end{aligned} \tag{30}$$

At the semipermeable wall ($Y = 1$), the solute flux is

$$J = V_{Y=1}(\bar{C}+C')-\frac{1}{\varepsilon Pe}\frac{\partial C'}{\partial Y}|^{Y=1}, \tag{31}$$

where $V_{Y=1}$ is the transverse flow velocity at the semipermeable wall ($Y = 1$) and $\partial C'/\partial Y|^{Y=1}$ is the concentration gradient in the y direction there.

For a solute that cannot permeate the wall, we have $J = 0$. Applying this boundary condition to Eq. 6 [10]. Neglecting C' in the first term (because $\bar{C} \gg C'$), the leading-order boundary condition gives

$$\partial C'/\partial Y|^{Y=1} = V|_{Y=1}\varepsilon Pe\bar{C}, \tag{32}$$

and Eq. 30 becomes

$$\begin{aligned}\frac{\partial \bar{C}}{\partial T}+\left(\bar{U}+\varepsilon Pe\left(-\frac{2\bar{U}}{105}\frac{\partial \bar{U}}{\partial X}+(\frac{3}{35}-\frac{1}{15}\bar{U})V|_{Y=1}\right)\right)\frac{\partial \bar{C}}{\partial X}\\ =\frac{\varepsilon}{Pe}(1+\frac{2}{105}\bar{U}^2Pe^2)\frac{d^2\bar{C}}{dX^2}\\ +\left(V|_{Y=1}+\varepsilon Pe\left(-\frac{2}{5}V|_{Y=1}{}^2+\frac{1}{15}\bar{U}\frac{\partial V|_{Y=1}}{\partial X}\right)\right)\bar{C},\end{aligned} \tag{33}$$

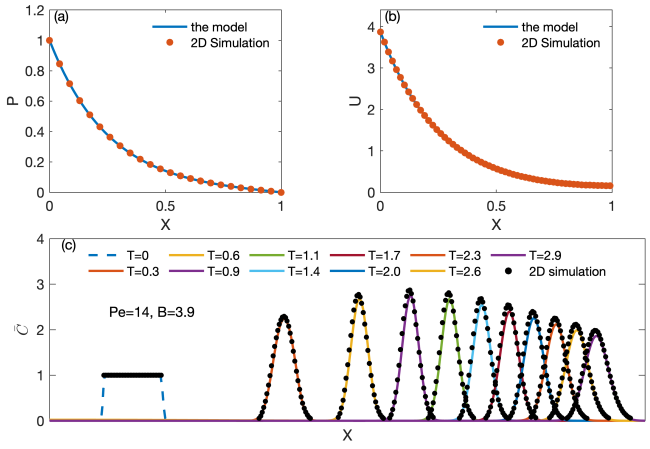

FIG. A1. **Comparison between the reduced order model and 2D COMSOL simulation** In the simulation, the rectangular channel has width 20 μm and length 5000 μm. The side walls have a permeability $k = 1\times10^{-15}$ m^2 and are separated by 5 µm. The viscosity is $7\times10^{-4}Pa\cdot s$, and the hydraulic conductivity is $\mathcal{L}_p = 2.86\times10^{-7}$ m/Pa/s. **(a,b)** The average pressure, varying axially, in the reduced-order model and the simulation. **(c)** The cross-sectionally averaged concentration profile, in the model and the simulation, with zero solute flux through the wall.

When $\varepsilon Pe \ll 1$, we can further simplify this equation by keeping only the leading-order term in the second advection term and the last source terms, respectively:

$$\frac{\partial \bar{C}}{\partial T}+\bar{U}\frac{\partial \bar{C}}{\partial X} = \frac{\varepsilon}{Pe}(1+\frac{2}{105}\bar{U}^2Pe^2)\frac{d^2\bar{C}}{dX^2}+V|_{Y=1}\bar{C}. \tag{34}$$

2. Validating the model with simulations

We performed two-dimensional simulations in COMSOL to validate the reduced model. A bolus, initially 500 μm wide and with uniform concentration, was placed at the inlet of a rectangular channel with width $2h = 20$ μm and length $L = 5000$ μm. With zero pressure at the outlet, a pressure $p_0 = 10$ Pa was applied at the inlet to drive flow. The hydraulic conductivity of the semipermeable walls was $\mathcal{L}_p = 2.86\times10^{-7}$ m Pa^{-1} s^{-1}. The fluid was water at 37°C ($\mu = 7\times10^{-4}$ Pa·s). The solute diffusivity was $D = 10^{-10}$ m^2/s. Thus, $\varepsilon = 0.002$, $B = 3.87$, and $Pe = 14.3$. The simulated pressure and velocity at the centerline ($Y = 0$) matched the reduced-order model well (Fig. A1a,b). The simulated, cross-sectionally averaged concentration profile varied over time and matched the reduced-order model well, showing that the bolus first became narrower and more concentrated, then became wider and more dilute (Fig. A1c).